Journal of Metals, Materials and Minerals, 35(4), e2358, 2025

Effect of lanthanum doping on phase transition, piezoelectric and energy storage properties of lead-free $0.93(Bi_{0.5}Na_{0.5})TiO_3$–$0.07BaTiO_3$ ceramics

Pathit PREMWICHIT[1], Songphop JAILA[1], and Sasipohn PRASERTPALICHAT[1,2,*]

[1] *Department of Physics, Faculty of Science, Naresuan University, Phitsanulok 65000, Thailand*
[2] *Research Center for Academic Excellence in Applied Physics, Faculty of Science, Naresuan University, Phitsanulok 65000, Thailand*

***Corresponding author e-mail**: sasipohnp@nu.ac.th

Received date:
16 March 2025
Revised date:
30 April 2025
Accepted date:
5 June 2025

Keywords:
BNBT lead-free piezoceramics;
A-site La doping;
Energy storage properties;
Piezoelectric properties

Abstract

In this study, lead-free $(Bi_{0.465}Na_{0.465}Ba_{0.07})_{(1-x)}La_xTiO_3$ (x=0.0–0.04) ceramics were synthesized using a conventional solid-state reaction method. All samples showed a single-phase perovskite structure with pseudocubic symmetry. The dense microstructure revealed a decrease in average grain size as x increased. La^{3+} addition stabilized polar nanoregions (PNRs), shifting the ferroelectric to relaxor phase transition temperature (T_{F-R}=104°C for x=0.0) to below room temperatures as La^{3+} content increased. This resulted in a transition from a rectangular to a relaxor-like thin P–E loop (x≥0.01), indicating a shift from ferroelectric (FE) to relaxor ferroelectric (RFE), which led to enhanced recoverable energy storage density (W_{rec}=0.55 J·cm^{-3} for x=0.01 and 0.02) and efficiency (η=75%) at x=0.03 under a 60 kV·cm^{-1} field. Additionally, the composition at x=0.01 achieved a maximum strain (S_{max}) of 0.21% with a high normalized strain (d^*_{33}) of 350 pm·V^{-1} under 60 kV·cm^{-1} at ambient temperature. These changes in the physical and electrical properties of the A-site doped BNT-based system are attributed to alterations in domain structure and defect chemistry

1. Introduction

Dielectric capacitors are important in electronic technologies, including medical ultrasonics, energy storage, pulse capacitors, advanced piezoelectric nanogenerator (PENGs), etc. [1-3]. The most widely used dielectric capacitors are lead-based materials, initially favored for their superior ferro/piezoelectric and energy storage properties, such as $Pb(Zr_{1-x}Ti_x)O_3$ [4] and $Pb_{1-x}La_x(Zr0.52Ti_{0.48})O_3$ [5]. However, lead-based systems are toxic and release harmful emissions during sintering [6], driving interest in lead-free ceramics. In 1961, Smolenskii *et al.* [7] discovered the lead-free piezoelectric material $Bi_{0.5}Na_{0.5}TiO_3$ (BNT), which was identified as a potential replacement for PZT due to its similar electronic configuration ($6s^2$) of Bi to Pb and its high Curie temperature (T_c=320°C), large remanent polarization (P_r=38 μC·cm^{-2}) and high coercive field (E_c~73 kV·cm^{-1}) at room temperature [8]. However, pure BNT ceramics face limitations like low insulation, poling challenges, high dielectric losses, and strong ferroelectricity, which hinder their piezoelectric and energy storage performance [9-10].

To expand BNT ceramics' applications, BNT is modified with $BaTiO_3$ (BT), forming a solid solution with morphotropic phase boundary (MPB) at BT content around ~6 mol% to 8 mol%, which separates the rhombohedral (BNT) and tetragonal (BT) phases [11]. This MPB improves various properties, including an increase in P_r to ~36 μC·cm^{-2}, d_{33} to ≥130 pC·N^{-1}, dielectric constant (~6000), strain (~0.15%), along with a reduction in E_c to ~28 kV·cm^{-1} and Q_m [12]. However, energy storage performance remains low due to a square P–E hysteresis loop, making slender P–E loops at room temperature challenging [13]. In 2011, Gao *et al.* [14] studied the energy storage performance of ceramics and found that doping $K_{0.5}Na_{0.5}NbO_3$ into $(1-x)(Bi_{0.5}Na_{0.5}TiO_3)$–$xBaTiO_3$ (denoted as $(1-x)$BNT–xBT, where x is 0.06) transformed the FE phase to a dispersed AFE phase at 20°C to 90°C, achieving W~0.59 J·cm^{-3} under 5.6 kV·mm^{-1}. Additionally, BNT–BT–KNN ternary compounds exhibit large strains (~0.4%), suggesting that composition and chemical modifier selection are key to optimizing properties [15]. Recent studies indicate that adding small amounts of dopants at the A/B sites in $(1-x)$BNT–xBT enhances both electrical and energy storage properties.

Lanthanum (La^{3+}) is a rare earth element widely used as a chemical modifier to enhance both the electrical and energy storage properties of ferroelectric ceramics. For example, Li *et al.* [16] found that La^{3+} doping in 0.94BNT–0.06BT ceramics decreased ferroelectric properties, enhancing energy storage performance (1.66 J·cm^{-3} at 105 kV·cm^{-1} for x = 0.05) and strain properties (0.53% with d^*_{33} of 707 pm·V^{-1} at 75 kV·cm^{-1} for x = 0.03). Similarly, Liu *et al.* [17] showed that La addition converted 0.95BNT–0.05BT from normal ferroelectric to a relaxor states, with non-ergodic relaxors (x=0.02) showing the highest piezoelectricity (151 pC·N^{-1}) and ergodic relaxors (x=0.04) displaying maximum strain (0.35% at 70 kV·cm^{-1}). With higher La content (x= 0.06–0.10), thin P–E loops were observed along with reducing loss tangent over the 100°C to 350°C range, which are crucial for enhancing energy storage density, and efficiency.

Although the composition range of x=0.06–0.07 has been identified as the MPB of $(1-x)$BNT–xBT, previous research has demonstrated that 0.93BNT–0.07BT possesses advantageous properties, including ferroelectrics (i.e., thinner P–E loops, lower coercive field (E_c), higher

polarization), and enhanced dielectric permittivity—the properties conducive to improved energy storage performance and electric-field-induced strain [18,19]. Moreover, there are few reports on the addition of La^{3+} in 0.93BNT–0.07BT ceramic systems compared to those on the 6% BT MPB composition (i.e., 0.94BNT–0.06BT). Therefore, this study investigates the effects of La^{3+} doping at the A-site of 0.93BNT–0.07BT, which is expected to induce relaxor behavior, refine grain morphology, and enhance dielectric, piezoelectric [16,17], and energy storage properties. A systematic investigation of the crystal structure, microstructure, dielectric, ferroelectric, energy storage, and piezoelectric properties of $(Bi_{0.465}Na_{0.465}Ba_{0.07})_{(1-x)}La_xTiO_3$ (x=0.0-0.04) ceramics has been conducted to gain a deeper understanding on their characteristics. The insight obtained from this study may contribute to the future development of lead-free ceramics with enhanced energy storage performance and electric-field-induced strain, which are potentially relevant for several applications as mentioned previously.

2. Experimental procedure

Lead-free $(Bi_{0.465}Na_{0.465}Ba_{0.07})_{(1-x)}La_xTiO_3$ (denoted as BNBT–xLa, where x is 0.0, 0.01, 0.02, 0.03, and 0.04) ceramics were prepared via the conventional solid-state reaction method, using Bi_2O_3 (99.9% Sigma-Aldrich), Na_2CO_3 (99.95% to 100.05%, Alfa Aesar), La_2O_3 (99.98%, Fluka, Analytical), $BaCO_3$ (99.8%, Alfa Aesar), and TiO_2 (≥99.9% Sigma-Aldrich) as starting raw materials. The raw materials were weighed according to their stoichiometric formula and ball-milled for 24 h in 99.9% ethanol with 10 mm diameter zirconia balls. The dried slurry was then pulverized and calcined at 800°C for 2 h, after which the milling process was repeated. Polyvinyl butyral (PVB) resin (3% by weight) was mixed with the dry powder as a binder, and the powder was pressed into disc-shaped pellets with a thickness of 1 mm to 2 mm and a diameter of approximately 15 mm. The pellets were placed in a crucible and covered with powder to reduce the volatilization of Na and Bi. Finally, they were heated at 400°C for 3 h to remove the PVB binder, followed by sintering at 1175°C (for x=0.0) and 1200°C (for x=0.01–0.04) for 2 h in an air atmosphere.

The phase purity of the sintered ceramics was investigated using X-ray diffraction (XRD, Bruker D8 Advance) over a 2θ range of 20° to 80°. The density of the ceramics was measured using the Archimedes method. The mirror-polished surfaces of the samples were thermally etched at approximately 100°C below the sintering temperature for 30 min, and then analyzed using a Field emission scanning electron microscope (FESEM, Thermo Scientific Apreo S). Before electrical property analysis, the ceramics were polished to a thickness of ~0.6 mm to 0.9 mm and coated with silver electrodes (Infinity Advanced Materials) on both sides, followed by firing at 700°C for 30 min. Before analysis, all samples were poled in silicone oil using a DC electric field of 55 $kV{\cdot}cm^{-1}$ for 20 min. The temperature dependence of the dielectric properties was measured with an LCR meter (HP 4284A) at frequencies of 1 kHz, 10 kHz, and 100 kHz over a wide temperature range of ~32°C to 450°C. Finally, the P–E hysteresis loop analysis was obtained using a ferroelectric testing system (Premier II, Radiant Technologies Inc., USA) at room temperature, with a measurement frequency of 1 Hz. Data from approximately 3 samples were averaged to ensure accuracy and reproducibility.

3. Results and discussion

Figure 1 shows the XRD patterns measured within the 2θ range of 20° to 80° for powders obtained by crushing the sintered BNBT–xLa (x=0.0–0.04) ceramics. All samples displayed pure perovskite structures with no impurity phases, suggesting that the La^{3+} ions could completely diffuse into the A-site of 0.93BNT–0.07BT, which confirms a homogeneous solid solution [21] within the resolution of the XRD instrument used. Figure 1(b–c) presents enlarged images of the XRD peaks of (111) and (200) planes in the 2θ range of ~39.9° and ~46.5°, respectively. These patterns demonstrate that La^{3+} ion doping does not significantly affect the phase structure, which consistently exhibited a single, relatively symmetrical peaks, suggesting a pseudocubic structure in all samples [16]. In addition, the (111) and (200) diffraction peaks were observed to shift towards higher diffraction angles as x increased, indicating a lattice contraction due to the relatively small ionic radius of La^{3+} ($r_{La^{3+}}$=1.36 Å) substituting the larger ions at the A-site (r_{Bi}=1.38 Å, r_{Na}=1.39 Å, r_{Ba}=1.61 Å) [22]. This result is consistent with previous studies on the 0.94BNT–0.06BT systems modified with La^{3+} [16], or the 0.88BNT–0.12BT systems modified with $(Li_{0.5}Nd_{0.5})$ [23], which exhibit similar behavior.

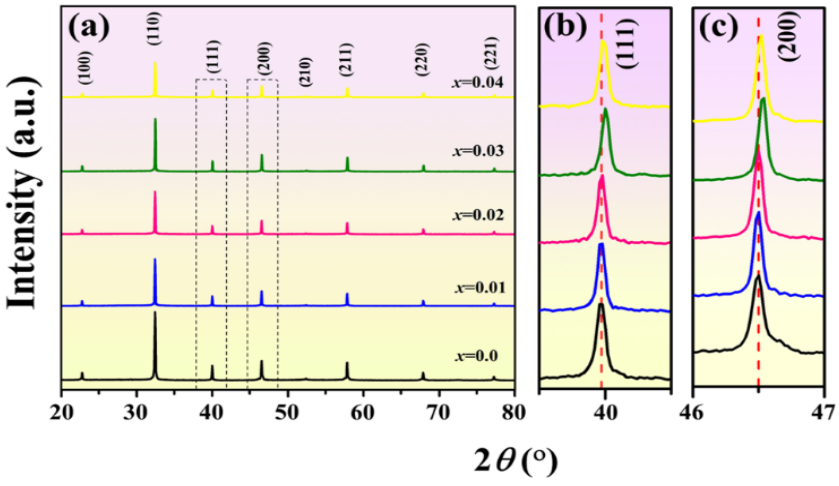

Figure 1. (a) X-ray diffraction patterns of BNBT–xLa (x=0.0–0.04) sintered and crushed, measured in the 2θ range of 20° to 80°, (b) ~39.9°, and (c) 46° to 47°.

The surface morphology of BNBT–*x*La (*x*=0.0–0.04) ceramics, which was polished and thermally corroded at 1,125°C for 30 min, is shown in Figure 2(a–e). With increasing *x*, the compositions showed an increase in density from 5.38 g·cm^{-3} (for *x*=0.0) to 5.46 g·cm^{-3}, 5.50 g·cm^{-3}, 5.54 g·cm^{-3} (for *x*=0.01, 0.02 and 0.03, respectively), then slightly decreased to 5.52 g·cm^{-3} for *x*=0.04, as confirmed by the Archimedes method. A dense microstructure, consisting of a mixture of large and small grains with distinct grain boundaries, was observed for all compositions. Reduced porosity was evident after La addition, which is consistent with the increase in density as *x* increased. The statistical analysis of the average grain size in FESEM of La^{3+}-doped 0.93BNT–0.07BT ceramic grains, determined using the linear intercept method, showed a significant decrease from 1.07 μm (for *x*=0.0) to 0.91 μm for *x*=0.02, before slightly increasing to 0.96 μm and 0.98 μm for *x*=0.03 and 0.04, respectively, as shown in Figure 2(a–e). The changes in average grain size, which initially showed a decrease with increasing *x*, could be ascribed to the defect chemistry alterations induced by La doping. During the high-temperature sintering process, volatile Bi_2O_3 and Na_2O are likely to evaporate, which leads to the formation of oxygen vacancies ($V_0^{\bullet\bullet}$), as described by the defect reaction in Equation (1–2) [24]:

$$2Bi_{Bi}^{X} + 3O_0^{X} \rightarrow 2V_{Bi}^{'''} + 3V_0^{\bullet\bullet} + Bi_2O_3 \quad (1)$$

$$2Na_{Na}^{X} + O_0^{X} \rightarrow 2V_{Na}^{'} + V_0^{\bullet\bullet} + Na_2O \quad (2)$$

These vacancies promote mass transfer, facilitating grain growth during sintering [25]. When doping La_2O_3 donor dopant into the A-site, it is expected to compensate the oxygen vacancies, as shown in Equation (3).

$$La_2O_3 + V_0^{\bullet\bullet} \xrightarrow{AO} 2La_A^{\bullet} + 3O_0^{X} \quad (3)$$

Therefore, the movement of grain boundaries is impeded, inhibiting grain growth and leading to a decrease in grain size [26]. As the La^{3+} content increases, the grain size gradually grows. This may be attributed to the smaller ionic radius of La^{3+} (1.36 Å) compared to the A-site ions (r_{Bi}=1.38 Å, r_{Na}=1.39 Å, r_{Ba}=1.61 Å). The smaller ionic radius of La^{3+} facilitates ion movement during the sintering process, leading to an increased atomic diffusion rate and promoting grain growth. Similar results have been reported in La^{3+}-modified $Bi_{0.5}Na_{0.5}TiO_3$-based ceramics [27,28].

The dielectric constant (ε_r) and dielectric loss (tanδ), measured at temperatures ranging from 29°C to 450°C and frequencies of 1 kHz, 10 kHz, and 100 kHz for poled BNBT–*x*La (*x*=0.0–0.04) ceramics, are shown in Figure 3(a–e). The BNBT–*x*La ceramics exhibited two distinct abnormal peaks in ε_r at $T_{F\text{-}R}$ and T_m. The first peak corresponds to the ferroelectric-to-relaxor ($T_{F\text{-}R}$) phase transition, and the second peak corresponds to the maximum dielectric constant at high temperature (T_m), approximately 300°C at 1 kHz, resulting from two combined mechanisms—the *R3c–P4bm* phase transition and the evolution of the *P4bm* phase with temperature [29]. From Figure 3(a–e), it is observed that $T_{F\text{-}R}$ for *x*=0.0 is at 104°C, and then the $T_{F\text{-}R}$ shifted to lower temperatures with increasing *x* content. Similarly, T_m decreased from 321°C (for *x*=0.0) to 281°C (for *x*=0.04), as shown in Table 1. La^{3+} doping at the A-site promotes the formation of polar nano-regions (PNRs), breaking the ferroelectric long-range order into a short-range relaxor phase with randomly distributed PNRs. This shifts $T_{F\text{-}R}$ to near or below ambient temperature, transitioning from a non-ergodic to an ergodic relaxor state. Additionally, T_m decreased and gradually flattened and broadened with La^{3+} doping, indicating a diffuse phase transition in the ceramic [21,30]. As the stability of the ferroelectric phase decreased, the maximum dielectric constant (ε_m) rapidly decreased from 4,788 (for *x*=0.0) to 2,963 (for *x*=0.04) with increasing *x*, while ε_r increased significantly from 889 (for *x*=0.0) to 1,689, 1,592, 1,297, and 1,535 for *x*=0.01, 0.02, 0.03, and 0.04, respectively. In addition, as the amount of La^{3+} doping increased, the dielectric loss (tanδ) values at temperatures ranging from 100°C to 363°C showed a decreasing trend, as shown in Table 1. It is well known that the t*an*δ value in the high-temperature range is due to the free charges (space charges) present in the sample. Thus, the decrease in tanδ with increasing La^{3+} content is likely attributed to reduced oxygen vacancies and various free charges [31].

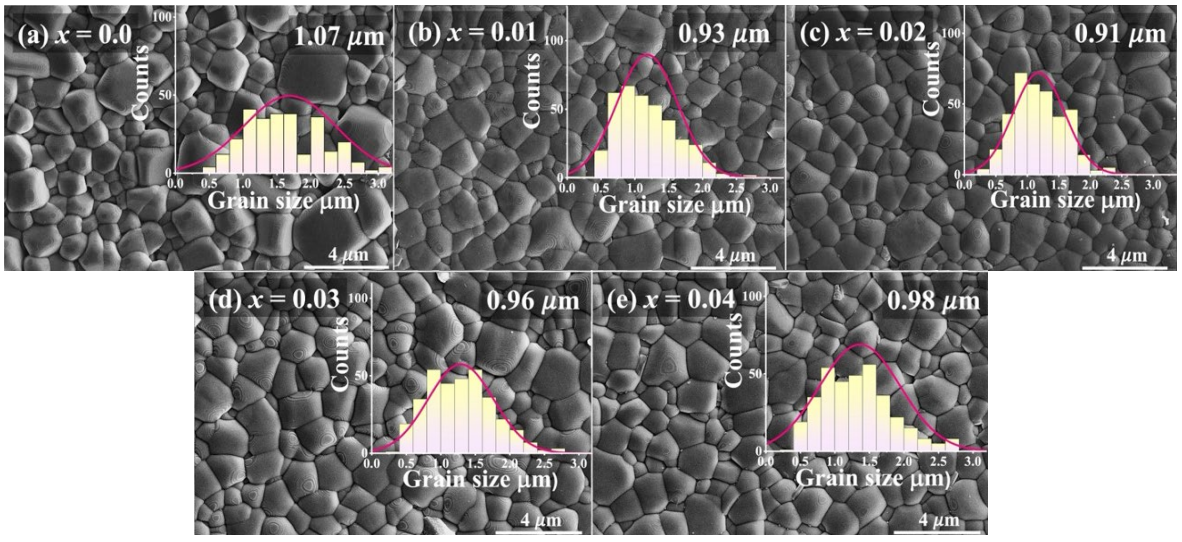

Figure 2. (a)–(e) FESEM images of the mirror-like surfaces of BNBT–*x*La (*x*=0.0–0.04) ceramics after thermal etching, with the insets illustrating the distribution of grain sizes.

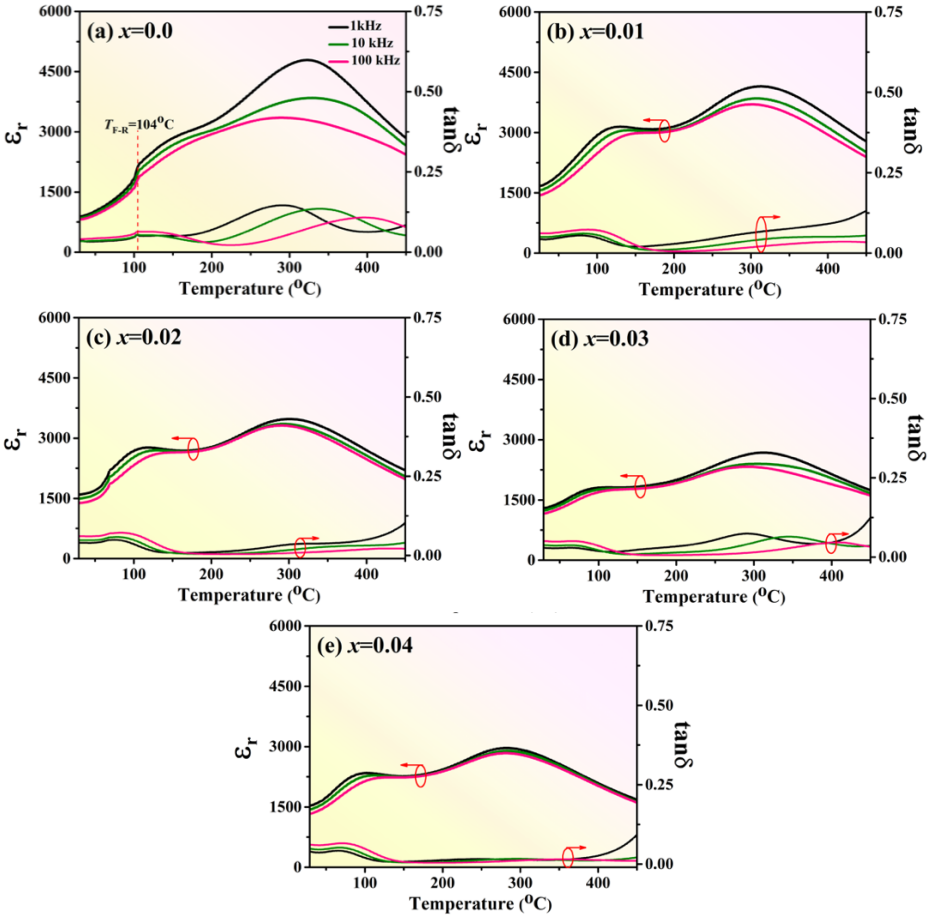

Figure 3. (a)–(e) Temperature dependences of the dielectric constant (ε_r) and dielectric loss (tanδ) of poled BNBT–xLa (x=0.0–0.04) ceramics measured at the frequency of 1 kHz, 10 kHz and 100 kHz.

Table 1. The dielectric property parameters of BNBT–xLa (x=0.0–0.04) ceramics at a measurement frequency of 1 kHz.

Compositions	$T_{F\text{-}R}$ [°C]	T_m [°C]	ε_r	tanδ_{RT}	ε_m	tanδ_m
x=0.0	104	321	889	0.039	4,788	0.127
x=0.01	<25	311	1,689	0.043	4,149	0.066
x=0.02	<25	301	1,592	0.040	3,474	0.034
x=0.03	<25	312	1,297	0.029	2,677	0.067
x=0.04	<25	281	1,535	0.038	2,963	0.014

The bipolar $P-E$ curves of BNBT–xLa (x=0–0.04) ceramics at ambient temperature were measured at a frequency of 1 Hz under an electric field of 60 kV·cm^{-1}, as shown in Figure 4(a–e). For x=0.0, the hysteresis loop exhibits a rectangular shape with relatively high values of coercive field and remanent polarization (E_c=28.77 kV·cm^{-1} and P_r = 28.07 μC·cm^{-2}), which is characteristic of conventional ferroelectrics and indicates a non-ergodic relaxor (NER) state. In this state, polar nanoregions (PNRs) are dynamically frozen and switch permanently to a stable ferroelectric phase, leading to high remnant polarization and low energy storage efficiency [32]. With increasing La^{3+} content, the $P-E$ hysteresis loop became thinner and narrower, with P_r decreasing nearly to zero, from 28.07 μC·cm^{-2} (at x=0.0) to 0.50 μC·cm^{-2} (at x=0.04). Similarly, E_c and P_{max} decreased significantly with increasing x content, as shown in Figure 4 and Table 2. These behaviors indicate that La^{3+} doping at the A-site enhances the relaxor behavior of 0.93BNT–0.07BT ceramics, aligning with the dielectric results from the previous section, which showed that the ferroelectric-to-relaxor phase transition temperature (T_{F-R}) decreased with increasing La^{3+} content. This indicates a transition to the ergodic relaxor (ER) phase, where dynamic PNRs can switch between the relaxor state and a long-range ferroelectric order under an applied electric field, and revert once the field is removed [32]. This yields a slimmer P–E loop with lower P_r and high P_{max} under the field. This reversible field-induced phase transition enhances both energy storage density and recoverable strain [33]. The reductions in P_r and E_c and the slight decrease in P_{max} are key factors that significantly enhance the energy storage properties of BNBT–xLa (x=0.0–0.04) ceramics.

The energy storage properties, including the recoverable energy storage density (W_{rec}) and energy storage efficiency (η), are shown in Table 2. Theoretically, ceramic capacitors' energy storage density and efficiency can be calculated using Equations (4–6) below [34].

$$W = \int_0^{P_{max}} EdP \quad (4)$$

$$W_{rec} = \int_{P_r}^{P_{max}} EdP \quad (5)$$

$$\eta = \frac{W_{rec}}{W_{rec} + W_{loss}} \times 100\% \quad (6)$$

Here, W, W_{loss}, and E represent the total energy storage density, energy storage density loss, and electric field, respectively. For the energy storage properties at x=0.0, the energy storage density and efficiency were relatively low due to the high P_r value of the ceramic, which resulted in a relatively high W_{loss} value of 1.79 J·cm^{-3}. Consequently, the x=0.0 is not yet suitable for energy storage applications. With increasing La^{3+} doping, the W_{rec} and η values gradually increased from 0.13 J·cm^{-3} and 7% (for x=0.0) to 0.55 J·cm^{-3} (for x=0.01 and 0.02) and 53%, 60%, and 75% for x=0.01, 0.02, and 0.03, respectively. The study found that the highest W_{rec} values were achieved at x=0.01 and 0.02, while η reached a maximum of 75% for x=0.03, as shown in Table 2. At x=0.04, W_{rec} and η decreased slightly to 0.50 J·cm^{-3} and 72%. The increase in W_{rec} and η was attributed to the low P_r and W_{loss} values, significantly enhancing these properties. Additionally, La^{3+} doping at the A-site significantly improved W_{rec} and η, consistent with previous studies on La-modified $Bi_{0.5}Na_{0.5}TiO_3$-based ceramics [16,35,36].

The bipolar strain hysteresis loops of BNBT–xLa (x=0.0–0.04) ceramics, measured at 60 kV·cm^{-1} under ambient temperature, are shown in Figure 5(a–e). For x=0.0, the S–E curve showed a saturated butterfly shape with a positive maximum strain (S_{max}) of 0.18% and a negative strain (S_{neg}) of 0.076%, as shown in Figure 5(a). As the La^{3+} content increased, the S–E curve gradually shifted from a butterfly shape to a sprout shape, with S_{neg} decreasing to zero at x≥0.01, indicating a relaxation behavior [37]. The maximum strain S_{max} of 0.21% occurs at x=0.01 before decreasing with further increases in x, as shown in Figure 5(b–e) and Table 2. The normalized piezoelectric coefficient (d_{33}*) is calculated as $d_{33}^* = S_{max}/E_{max}$. The results align with S_{max}, reaching a maximum of 350 pm·V^{-1} at x=0.01 before gradually decreasing with further increasing x, as shown in Table 2. The decreases in S_{max} and d_{33}* indicate a transition from the ferroelectric to the relaxor phase in the ceramic at ambient temperature [38,39].

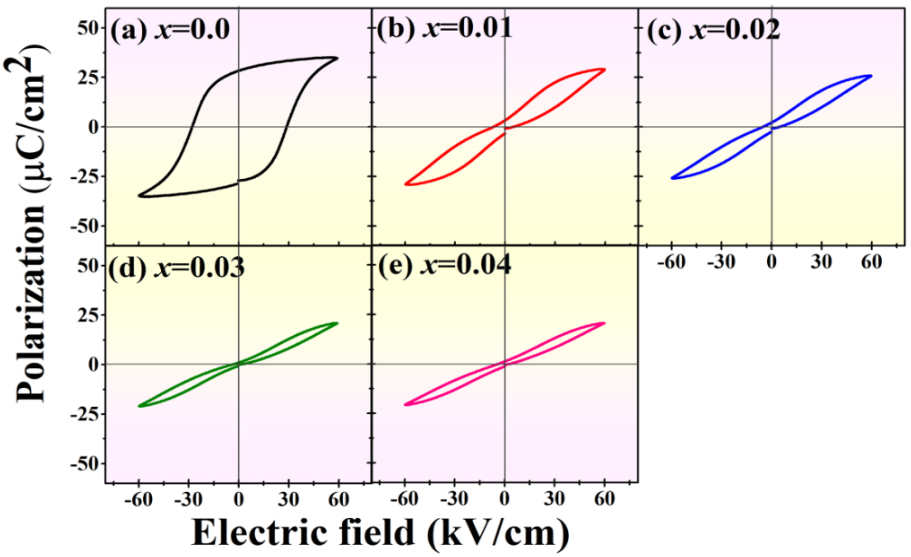

Figure 4. The bipolar P–E loops of the BNBT–xLa ceramics at ambient temperature for (a) x=0.0, (b) x=0.01, (c) x=0.02, (d) x=0.03, and (e) x=0.04.

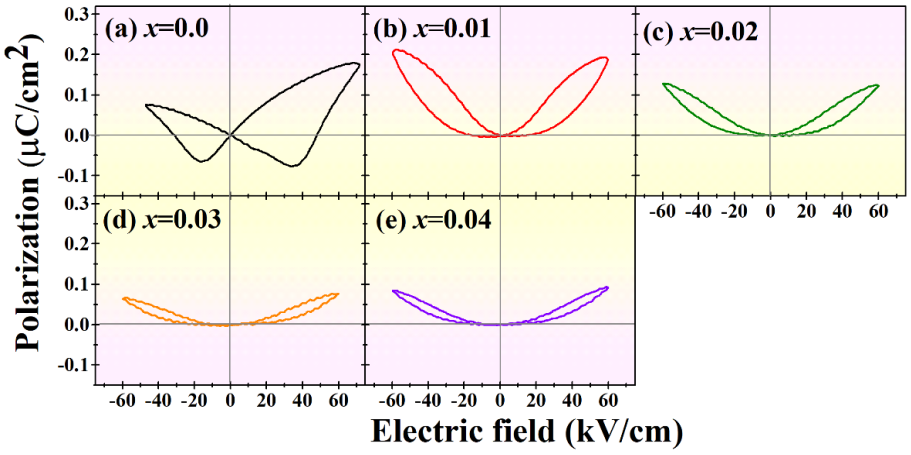

Figure 5. The bipolar S–E curve of the BNBT–xLa ceramics at ambient temperature for (a) x=0.0, (b) x=0.01, (c) x=0.02, (d) x=0.03, and (e) x=0.04.

Table 2. Ferroelectric, energy storage, and strain property of BNBT–xLa (x=0.0–0.04) ceramics at a measurement frequency of 1 Hz.

Compositions	E_c [kV·cm^{-1}]	P_r [μC·cm^{-2}]	P_{max} [μC·cm^{-2}]	W [J·cm^{-3}]	W_{rec} [J·cm^{-3}]	W_{loss} [J·cm^{-3}]	η [%]	S_{max} [%]	S_{neg} [%]	(d^*_{33}) [pm·V^{-1}]
x=0.0	28.77±1.75	28.07±1.42	35.16±0.58	1.92±0.10	0.13±0.02	1.79±0.08	7±1	0.18±0.01	0.076±0.01	300±17
x=0.01	3.83±0.65	2.91±0.56	29.16±0.21	1.04±0.05	0.55±0.01	0.49±0.06	53±3	0.21±0.01	0	350±17
x=0.02	1.88±0.46	2.13±0.6	25.89±0.06	0.91±0.04	0.55±0.01	0.36±0.02	60±2	0.13±0.01	0	216±16
x=0.03	1.12±0.25	0.87±0.6	21.02±0.43	0.71±0.02	0.53±0.01	0.18±0.01	75±2	0.07±0.01	0	116±16
x=0.04	1.03±0.78	0.50±0.25	20.64±0.17	0.70±0.01	0.50±0.01	0.20±0.01	72±2	0.09±0.01	0	150±17

4. Conclusion

The effects of La^{3+} doping at the A-site on the crystal structure, microstructure, and electrical properties of $(Bi_{0.465}Na_{0.465}Ba_{0.07})_{(1-x)}La_xTiO_3$ (x=0.0–0.04) ceramics were studied. Ceramics were synthesized via solid-state reaction, with calcination at 800°C and sintering at 1,175°C to 1,200°C for 2 h. XRD confirmed a pure pseudo-cubic perovskite phase. Increasing La^{3+} content raised density (5.38 g·cm^{-3} to 5.54 g·cm^{-3}) and decreased average grain size from 1.07 μm (x=0.0) to 0.91 μm at (x=0.02), with slight increases at higher doping levels. $T_{F\text{-}R}$ dropped below room temperature for $x \geq 0.01$, indicating enhanced relaxation behavior, while T_m decreased from 321°C to 281°C. With increased relaxation, the P–E loop thinned, with P_r dropping to zero at x=0.04. This resulted in W_{rec} up to 0.55 J·cm^{-3} for x=0.01–0.02 and η of 75% at x=0.03. At x=0.01, the S–E loop shifted to a sprout shape, indicating an ergodic relaxor state, with S_{max} of 0.21% at 60 kV·cm^{-1} and $d_{33}{}^*$ of 350 pm·V^{-1}. These findings showcase BNBT–xLa ceramics as a promising candidate for lead-free piezoelectric energy storage.

Acknowledgment

This work was supported by Naresuan University (NU), and National Science, Research and Innovation Fund (NSRF), Grant NO. R2567B075. Partial support was also provided by the Global and Frontier Research University Fund, Naresuan University, Grant NO. R2567C001. The authors would like to express their gratitude to the Department of Physics, Faculty of Science, Naresuan University, for providing research facilities. Special thanks are also extended to Dr. Nitish Kumar for his assistance with grammar checking and proofreading.

References

[1] L. Yang, X. Kong, F. Li, H. Hao, Z. Cheng, H. Liu, J.-F. Li, and S. Zhang, "Perovskite lead-free dielectrics for energy storage applications," *Progress in Materials Science*, vol. 102, pp. 72-108, 2019.

[2] D. Damjanovic, and R. Newnham, "Electrostrictive and piezoelectric materials for actuator applications," *Journal of Intelligent Material Systems and Structures*, vol. 3, pp. 190-208, 1992.

[3] J. Lee, S. Hajra, S. Panda, W. Oh, Y. Oh, H. Shin, Y. K. Mishra, and H. J. Kim, "Accelerate the shift to green energy with PVDF based piezoelectric nanogenerator," International *Journal of Precision Engineering and Manufacturing-Green Technology*, vol. 11, pp. 233-241, 2024.

[4] R. Guo, L. Cross, S. Park, B. Noheda, D. Cox, and G. Shirane, "Origin of the high piezoelectric response in $PbZr_{1-x}Ti_xO_3$," *Physical Review Letters*, vol. 84, p. 5423, 2000.

[5] H. T. Dang, T. T. Trinh, C. T. Nguyen, T. V. Do, M. D. Nguyen, and H. N. Vu, "Enhancement of relaxor behavior by La doping and its influence on the energy storage performance and electric breakdown strength of ferroelectric $Pb(Zr_{0.52}Ti_{0.48})O_3$ thin films," *Materials Chemistry and Physics*, vol. 234, pp. 210-216, 2019.

[6] K. J. Puttlitz, and G. T. Galyon, "Impact of the ROHS directive on high-performance electronic systems, in: Lead-free electronic solders," Springer, 2006, pp. 347-365.

[7] G. A. Smolenskii, V. A. Isupo, A I. Agranovskaya, and N. N. Krainik, "New ferroelectrics of. complex composition," *Soviet physics. Solid state*, vol. 2, pp. 2651-2654, 1961'.

[8] T. Takenaka, K. M. K. Maruyama, and K. S. K. Sakata, "$(Bi_{1/2}Na_{1/2})TiO_3$-$BaTiO_3$ system for lead-free piezoelectric ceramics," *Japanese Journal of Applied Physics*, vol. 30, p. 2236, 1991.

[9] M. Benyoussef, M. Zannen, J. Belhadi, B. Manoun, J.-L. Dellis, M. El Marssi, and A. Lahmar, "Dielectric, ferroelectric, and energy storage properties in dysprosium doped sodium bismuth titanate ceramics," *Ceramics International*, vol. 44, pp. 19451-19460, 2018.

[10] Y. Hiruma, H. Nagata, T. Takenaka, Thermal depoling process and piezoelectric properties of bismuth sodium titanate ceramics, J*ournal of Applied Physics*, vol. 105, 2009.

[11] Y. Saito, H. Takao, T. Tani, T. Nonoyama, K. Takatori, T. Homma, T. Nagaya, and M. Nakamura, "Lead-free piezoceramics," *Nature*, vol. 432, pp. 84-87, 2004.

[12] A. Prado, L. Ramajo, J. Camargo, A. del Campo, P. Öchsner, F. Rubio-Marcos, and M. Castro, "Stabilization of the morphotropic phase boundary in $(1-x)Bi_{0.5}Na_{0.5}TiO_3$–$xBaTiO_3$ ceramics through two alternative synthesis pathways," *Journal of Materials Science: Materials in Electronics*, vol. 30, pp. 18405-18412, 2019.

[13] L. Zheng, X. Yi, S. Zhang, W. Jiang, B. Yang, R. Zhang, and W. Cao, "Complete set of material constants of $0.95(Na_{0.5}Bi_{0.5})TiO_3$-$0.05BaTiO_3$ lead-free piezoelectric single crystal and the delineation of extrinsic contributions," *Applied Physics Letters*, vol.103, 2013.

[14] F. Gao, X. Dong, C. Mao, W. Liu, H. Zhang, L. Yang, F. Cao, and G. Wang, "Energy-storage properties of $0.89Bi_{0.5}Na_{0.5}TiO_3$–$0.06BaTiO_3$–$0.05K_{0.5}Na_{0.5}NbO_3$ lead-free anti-ferroelectric ceramics," *Journal of the American Ceramic Society*, vol. 94, pp. 4382-4386, 2011.

[15] W. Jo, T. Granzow, E. Aulbach, J. Rödel, and D. Damjanovic, "Origin of the large strain response in $(K_{0.5}Na_{0.5})NbO_3$-modified

($Bi_{0.5}Na_{0.5}$)TiO_3–$BaTiO_3$ lead-free piezoceramics," *Journal of Applied Physics*, vol. 105, p. 094102, 2009.

[16] F. Li, Y. Liu, Y. Lyu, Y. Qi, Z. Yu, and C. Lu, "Huge strain and energy storage density of A-site La^{3+} donor doped ($Bi_{0.5}Na_{0.5}$)$_{0.94}Ba_{0.06}TiO_3$ ceramics," *Ceramics International*, vol. 43, pp. 106-110, 2017.

[17] X. Liu, H. Guo, and X. Tan, "Evolution of structure and electrical properties with lanthanum content in $[(Bi_{1/2}Na_{1/2})_{0.95}Ba_{0.05}]_{1-x}La_xTiO_3$ ceramics," *Journal of the European Ceramic Society*, vol. 34, pp. 2997-3006, 2014.

[18] A. Prado-Espinosa, J. Camargo, A. del Campo, F. Rubio-Marcos, M. Castro, and L. Ramajo, "Exploring new methodologies for the identification of the morphotropic phase boundary region in the (BiNa)TiO_3-$BaTiO_3$ lead free piezoceramics: Confocal Raman Microscopy," *Journal of Alloys and Compounds*, vol. 739, pp. 799805, 2018.

[19] A. Prado, L. Ramajo, J. Camargo, A. del Campo, P. Öchsner, F. Rubio-Marcos, and M. Castro, "Stabilization of the morphotropic phase boundary in $(1-x)Bi_{0.5}Na_{0.5}TiO_3$–$xBaTiO_3$ ceramics through two alternative synthesis pathways," *Journal of Materials Science: Materials in Electronics*, vol. 30 , pp. 18405-18412, 2019.

[20] B. Jaffe, W. R. Cook Jr. and H. Jaffe, "Piezoelectric Ceramics," Academic Press, London and New York, 1971.

[21] L. Li, M. Xu, Q. Zhang, P. Chen, N. Wang, D. Xiong, B. Peng, and L. Liu, "Electrocaloric effect in La-doped BNT-6BT relaxor ferroelectric ceramics," *Ceramics International,* vol. 44, pp. 343-350, 2018.

[22] L. Pauling, "The nature of the chemical bond and the structure of molecules and crystals: An introduction to modern structural chemistry," *Cornell university press*, 3rd edition by Pauling, Linus, 1960.

[23] C. Zhou, Q. Li, J. Xu, L. Yang, W. Zeng, C. Yuan, and G. Chen, "Ferroelectric-quasiferroelectric-ergodic relaxor transition and multifunctional electrical properties in $Bi_{0.5}Na_{0.5}TiO_3$-based ceramics," *Journal of the American Ceramic Society*, vol. 101, pp. 1554-1565, 2018.

[24] R. A. Malik, A. Hussain, A. Maqbool, A. Zaman, T. K. Song, W.-J. Kim, andM.-H. Kim, "Giant strain, thermally-stable high energy storage properties and structural evolution of Bi-based lead-free piezoceramics," *Journal of Alloys and Compounds*, vol. 682, pp. 302-310, 2016.

[25] R. Machado, V. B. dos Santos, D. A. Ochoa, E. Cerdeiras, L. Mestres, and J. E. García, "Elastic, dielectric and electro-mechanical properties of ($Bi_{0.5}Na_{0.5}$)TiO_3-$BaTiO_3$ piezoceramics at the morphotropic phase boundary region," *Journal of Alloys and Compounds*, vol. 690, pp. 568-574, 2017.

[26] X. Qiao, F. Zhang, D. Wu, B. Chen, X. Zhao, Z. Peng, X. Ren, P. Liang, X. Chao, and Z. Yang, "Superior comprehensive energy storage properties in $Bi_{0.5}Na_{0.5}TiO_3$-based relaxor ferroelectric ceramics," *Chemical Engineering Journal*, vol. 388, p. 2020 124158, 2020.

[27] P. Fu, Z. Xu, R. Chu, W. Li, G. Zang, and J. Hao, "Piezo- electric, ferroelectric and dielectric properties of La_2O_3-doped ($Bi_{0.5}Na_{0.5}$)$_{0.94}Ba_{0.06}TiO_3$ lead-free ceramics," *Materials & Design*, vol. 31, pp. 796-801, 2010.

[28] A. Ullah, Z. Yao, H. Liu, H. Hao, A. Manan, A. Ullah, A. Jan, M. Cao, S. Ahmad, and F. Alresheedi, "Improved energy storage properties of $La_{0.33}NbO_3$ modified 0.94$Bi_{0.5}Na_{0.5}TiO_3$-0.06$BaTiO_3$ ceramic system," *Applied Physics A*, vol. 127, pp. 1-12, 2021.

[29] W. Jo, S. Schaab, E. Sapper, L.A. Schmitt, H.-J. Kleebe, A.J. Bell, and J. Rödel, "On the phase identity and its thermal evolution of lead free ($Bi_{1/2}Na_{1/2}$)TiO_3-6 mol% $BaTiO_3$," *Journal of Applied Physics*, vol. 110, p. 074106, 2011.

[30] B. Ji, Q. Li, S. Zheng, Q. Li, W. Wang, and H. Fan, "Giant strain and excellent anti-fatigue properties of La^{3+} doped $(Na_{0.84}K_{0.16})_{0.5}Bi_{0.5}Ti_{0.985}Ta_{0.015}O_3$ lead-free ceramics," *Materials Science and Engineering: B*, vol. 305, p. 117439, 2024.

[31] P. Fu, Z. Xu, R. Chu, W. Li, G. Zang, and J. Hao, "Piezoelectric, ferroelectric and dielectric properties of Nd_2O_3-doped ($Bi_{0.5}Na_{0.5}$)$_{0.94}Ba_{0.06}TiO_3$ lead-free ceramics," *Materials Science and Engineering: B*, vol. 167, pp. 161-166, 2010.

[32] R. K. Sahu, K. Banerjee, and S. Asthana, "Ergodic-nonergodic relaxor behavior, recoverable energy storage density, and dynamic hysteresis scaling in NKBT ferroelectrics," *Journal of Materials Science: Materials in Electronics*, vol. 34, p. 972, 2023.

[33] A. Ullah, C. W. Ahn, A. Ullah, and I. W. Kim, "Large strain under a low electric field in lead-free bismuth-based piezo-electrics," *Applied Physics Letters*, vol. 103, p. 022906, 2013.

[34] N. Zhao, H. Fan, L. Ning, J. Ma, and Y. Zhou, "Temperature-stable dielectric and energy storage properties of La($Ti_{0.5}Mg_{0.5}$)O_3-doped ($Bi_{0.5}Na_{0.5}$)TiO_3-($Sr_{0.7}Bi_{0.2}$)TiO_3 lead-free ceramics," *Journal of the American Ceramic Society*, vol. 101, pp. 5578-5585, 2018.

[35] X. Zhang, Y. Xiao, B. Du, Y. Li, Y. Wu, L. Sheng, and W. Tan, "Improved non-piezoelectric electric properties based on a modulated ferroelectric-ergodic relaxor transition in ($Bi_{0.5}Na_{0.5}$) TiO_3-Ba(Ti, Zr)O_3 ceramics," *Materials*, vol. 14, p. 6666, 2021.

[36] Q. Li, W. Zhang, C. Wang, L. Ning, Y. Wen, B. Hu, and H. Fan, "Enhanced energy-storage performance of (1-x)(0.72$Bi_{0.5}Na_{0.5}TiO_3$-0.28$Bi_{0.2}Sr_{0.7\square0.1}TiO_3$)-$x$La ceramics," *Journal of Alloys and Compounds*, vol. 775, pp. 116-123, 2019.

[37] S. Pang, L. Yang, J. Qin, H. Qin, H. Xie, H. Wang, C. Zhou, and J. Xu, "Low electric field-induced strain and large improvement in energy density of $(Lu_{0.5}Nb_{0.5})^{4+}$ complex-ions doped BNT–BT ceramics," *Applied Physics A*, vol. 125, pp. 1-12, 2019.

[38] X. Liu, J. Zhai, B. Shen, F. Li, Y. Zhang, P. Li, and B. Liu, "Electric-field-temperature phase diagram and electromechanical properties in lead-free ($Na_{0.5}Bi_{0.5}$)TiO_3-based incipient piezoelectric ceramics," *Journal of the European Ceramic Society*, vol. 37, pp. 1437-1447, 2017.

[39] R. A. Malik, A. Hussain, A. Zaman, A. Maqbool, J. U. Rahman, T. K. Song, W.-J. Kim, and M.-H. Kim, "Structure–property relationship in lead-free A-and B-site co-doped $Bi_{0.5}(Na_{0.84}K_{0.16})_{0.5}TiO_3$–$SrTiO_3$ incipient piezoceramics," *RSC Advances*, vol. 5, pp. 96953-96964, 2015.